Chemical Engineering Journal 148 (2009) 533–538

Contents lists available at ScienceDirect

Chemical Engineering Journal

journal homepage: www.elsevier.com/locate/cej

Finite element solution of the fluid–solid reaction equations with structural changes

A. Afshar Ebrahimi[a,*], H. Ale Ebrahim[a], M. Hatam[b], E. Jamshidi[a]

[a] Department of Chemical Engineering, Amirkabir University of Technology (Tehran Polytechnic), Petrochemical Center of Excellency, Tehran 15875-4413, Iran
[b] Department of Mechanical Engineering, Fars Engineering Research Center, Shiraz, Iran

ARTICLE INFO

Article history:
Received 15 July 2008
Received in revised form 5 January 2009
Accepted 8 January 2009

Keywords:
Fluid–solid reactions
Random pore model
Modified grain model
Rayleigh–Ritz finite element method

ABSTRACT

The finite element solution for gas–solid reactions is developed to include fluid accumulation term in the solid pellet (liquid–solid reactions) accompanied with structural changes in the solid phase. In these reactions the fluid balance equation in the pellet is an unsteady state equation which is coupled with the solid phase equation. The fluid balance equation is analyzed numerically by the combination of Rayleigh–Ritz finite element method and finite difference approximation while the solid equation is solved by fourth order Runge–Kutta method simultaneously. This method shows flexible behavior in all reaction regimes even in the diffusion-limited regimes accompanied with significant structural changes. Equations of the modified grain model and random pore model are considered in this work. Finally results of this work are compared with some other existing solutions and experimental data successfully.

1. Introduction

Fluid–solid noncatalytic reactions have a pivotal role in the chemical and metallurgical industries [1–6]. The major steps involved in these reactions are the transport of the fluid reactants into the internal void space of the solid reactant, chemical reaction within the solid phase and transport of products from the particle interior to the particle surface.

The structural behavior of noncatalytic reactions is a function of the reaction products. In other words, when solid products are formed by the reaction, the structural changes depend on the ratio of the molar volumes of this products and solid reactant. Because of continuous evolution of the solid structure, noncatalytic fluid–solid reactions have sophisticated partial differential equations. In modeling fluid–solid reactions with structural changes, it is common to consider the reaction as occurring on internal surfaces of the solid. The models can be classified into two categories as follows:

Those that consider the reaction on the surfaces of nonporous grains. In other words the uniformly sized nonporous grains of the solid react with the fluid reactant in the shrinking core behavior [7–9].

Those that emphasize instead the reaction initiated on pore surfaces within the solid pellet (random pore models) [10–15], which consider the pore space as a bundle of randomly connected capillaries which have various sizes and orientations. Detailed descriptions of pore growth and pore combination have also been realized by population balance techniques [16–18]. In our previous work [19] equations of the quasi steady state gas–solid reactions without structural changes in the pellet were solved by finite element method. Also the solution of several gas–solid reaction models by orthogonal collocation method including structural and nonstructural changes has been done elsewhere [20].

In this paper the unsteady partial differential equation of the fluid balance in the particle is numerically analyzed by the combination of Rayleigh–Ritz finite element method and finite difference approximation while the solid equation is solved by the fourth order Runge–Kutta method simultaneously. The solution technique for the modified grain model is described in details. Other presented random pore model equations can be solved similarly. Some computer codes have been developed for this purpose in MATLAB media. This computer code is able to solve these equations with various mesh numbers with significant accuracy even in the presence of high gas concentration gradients accompanied with severe structural changes. Results of this work are compared with some existing solutions and experimental data successfully.

2. Mathematical modeling

Consider the following fluid–solid reaction:

$$A(\text{fluid}) + \upsilon_B B(\text{s}) \rightarrow C(\text{fluid}) + \upsilon_D D(\text{s}) \quad (1)$$

The following assumptions are used in the modeling:

1. The diffusion in the pellet is equimolar counter-diffusion.

* Corresponding author. Tel.: +98 21 64543198; fax: +98 21 66405847.
E-mail address: a.afshar@aut.ac.ir (A.A. Ebrahimi).

1385-8947/$ – see front matter © 2009 Elsevier B.V. All rights reserved.
doi:10.1016/j.cej.2009.01.009

2. The system is isothermal.
3. The pellet size is constant.
4. The reaction is irreversible and first order with respect to the gaseous reactant [2,7,11,13].

2.1. Random pore model

The dimensionless governing equations of the random pore model for a spherical pellet are as follows [10,11]:

$$\kappa\phi_r^2\frac{\partial a}{\partial\theta_r}=\frac{1}{y^2}\frac{\partial}{\partial y}\left(\delta y^2\frac{\partial a}{\partial y}\right)-\frac{\phi_r^2 ab\sqrt{1-\psi\ln b}}{1+\beta Z/\psi[\sqrt{1-\psi\ln b}-1]} \tag{2}$$

$$\frac{\partial b}{\partial\theta_r}=-\frac{ab\sqrt{1-\psi\ln b}}{1+\beta Z/\psi[\sqrt{1-\psi\ln b}-1]} \tag{3}$$

The initial and boundary conditions are expressed as

$$\theta_r=0,\quad b=1,\quad a=0 \tag{4}$$

$$y=0,\quad \frac{\partial a}{\partial y}=0 \tag{5}$$

$$y=1,\quad \frac{\partial a}{\partial y}=\frac{Sh}{\delta}(1-a) \tag{6}$$

Dimensionless parameters are defined in the notation. The parameter κ in Eq. (2) is normally small (i.e. $\kappa=0.01$ or less) for gas–solid systems, where κ can be as large as about 0.5 in liquid–solid systems [21]. Pore size distribution in this model is presented by the parameter ψ. Moreover, the structural changes parameter Z, and product layer resistance are also considered (β). For $Z>1$, the product layer molar volume is more than solid reactant and the porosity decreases with the progress of reaction. For $Z<1$ the product layer volume is less than solid reactant and porosity increases. Finally for $Z=1$, the pore size is unaffected by the reaction.

The porosity of the pellet at each time can be expressed as follows [7]:

$$\frac{\varepsilon}{\varepsilon_0}=1-\frac{(Z-1)(1-\varepsilon_0)(1-b)}{\varepsilon_0} \tag{7}$$

For relating pore diffusion to the pellet porosity two approaches exist. First approach is from Wakao and Smith [21] as follows:

$$\delta=\frac{D_e}{D_{e0}}=\left(\frac{\varepsilon}{\varepsilon_0}\right)^2=\left[1-\frac{(Z-1)(1-\varepsilon_0)(1-b)}{\varepsilon_0}\right]^2 \tag{8}$$

Second approach assumes that tortuosity factor of the pellet remains constant during the reaction. The result of this approach is as follows:

$$\delta=\frac{D_e}{D_{e0}}=\left(\frac{\varepsilon}{\varepsilon_0}\right)=\left[1-\frac{(Z-1)(1-\varepsilon_0)(1-b)}{\varepsilon_0}\right] \tag{9}$$

By Eqs. (8) or (9), the variation of pore diffusion with the progress of reaction can be considered. In this work Eq. (8) was used, unless otherwise specified.

In this model the solid conversion for a spherical pellet can be calculated by the following equation:

$$X(\theta)=1-3\int_0^1 y^2 b(\theta,\,y)\mathrm{d}y \tag{10}$$

2.2. Modified grain model

The dimensionless governing equations of the modified grain model for spherical pellet and spherical grains are as follows [22]:

$$\kappa\phi_g^2\frac{\partial a}{\partial\theta_g}=\frac{1}{y^2}\frac{\partial}{\partial y}\left(\delta y^2\frac{\partial a}{\partial y}\right)-\frac{\sigma^2 a r^{*2}}{1+6\sigma_g^2(r^*-(r^{*2}/r^{**}))} \tag{11}$$

$$\frac{\partial r^*}{\partial\theta_g}=-\frac{a}{1+6\sigma_g^2(r^*-r^{*2}/r^{**})} \tag{12}$$

$$r^{**}=[Z+(1-Z)r^{*3}]^{1/3} \tag{13}$$

$$Z=\frac{\upsilon_D\rho_B M_D}{\upsilon_B\rho_D M_B} \tag{14}$$

where the initial condition is as follows:

$$\theta_g=0,\quad r^*=1,\quad a=0 \tag{15}$$

The boundary conditions are similar to Eqs. (5) and (6).

In this model the solid conversion for a spherical pellet can be calculated by the following equation:

$$X(\theta)=1-3\int_0^1 y^2 r^{*3}(\theta,\,y)\mathrm{d}y \tag{16}$$

3. Finite element method

In this section the spherical solid pellet is divided to the uniform mesh from the center up to the surface of the sphere. Since the solid concentration is known at the initial time, the fluid concentration will be obtained by the combination of the Rayleigh–Ritz finite element method and finite difference approximation for the next time step while the grain radius (or solid concentration in random pore model) is being calculated for the next time step by fourth order Runge–Kutta method at each location in the pellet simultaneously. This procedure will be repeated until final reaction time. Consider a typical element $\Omega_e(y_a, y_b)$, whose endpoints have the coordinates $y=y_a$ and $y=y_b$, is isolated from the mesh. The weighted integral form of Eq. (11) is as follows:

$$4\pi\int_{y_a}^{y_b} w\left(\kappa\phi_g^2\frac{\partial a}{\partial\theta_g}-\frac{1}{y^2}\frac{\partial}{\partial y}\left(\delta y^2\frac{\partial a}{\partial y}\right)+\frac{\phi_g^2 a r^{*2}}{1+6\phi_g^2(r^*-(r^{*2}/r^{**}))}\right)y^2\,\mathrm{d}y=0 \tag{17}$$

where w denotes the weight function. Terms 4π and $y^2\,\mathrm{d}y$ in the above equation are due to spherical differential volume element of the pellet which its radius is denoted by y.

Integration by parts is used on the second term of Eq. (17) to distribute the spatial derivative equally between the weight function w and the dependent variable a:

$$-y^2 w\delta\frac{\partial a}{\partial y}+\int_{y_a}^{y_b}\left(y^2\delta\frac{\mathrm{d}w}{\mathrm{d}y}\frac{\mathrm{d}a}{\mathrm{d}y}+y^2 w\kappa\phi_g^2\frac{\partial a}{\partial\theta_g}+\frac{w y^2\phi_g^2 a r^{*2}}{1+6\phi_g^2(r^*-(r^{*2}/r^{**}))}\right)\mathrm{d}y=0 \tag{18}$$

Eq. (18) is the weak form of the differential equation. First term in the above equation is related to natural boundary conditions in the nodes of a typical element. The fluid concentration (dependent variable) in each mesh is defined as follows:

$$a(y,\theta)\approx\sum_{j=1}^{n} a_j^e(\theta)L_j^e(y) \tag{19}$$

where $L_j^e(y)$ are the one dimensional Lagrangian interpolation functions over an element. The nodal values of the fluid concentration $a_j^e(\theta)$ are functions of time only. The above approximation is called decoupled formulation in one-dimensional time-dependent problems in finite element method [23]. The value of n in Eq. (19) depends on the order of the employed interpolation functions. For

instance, $n=2$ in case of using linear interpolation functions and $n=3$ in case of employing quadratic interpolation functions respectively. Also the higher interpolation functions can be applied but the quadratic interpolation functions give the most accurate results in this work. The quadratic interpolation functions which are used in this work are as follows [23,24]:

$$L_1^e(\bar{y}) = \left(1 - \frac{2\bar{y}}{h}\right)\left(1 - \frac{\bar{y}}{h}\right), \quad L_2^e(\bar{y}) = \frac{4\bar{y}}{h}\left(1 - \frac{\bar{y}}{h}\right),$$
$$L_3^e(\bar{y}) = -\frac{\bar{y}}{h}\left(1 - \frac{2\bar{y}}{h}\right) \tag{20}$$

where $\bar{y}$ is the element or local coordinate.

In the Rayleigh–Ritz method we have [23]:

$$w = L \tag{21}$$

Substituting Eqs. (19) and (21) into Eq. (18) results in:

$$\int_{y_a}^{y_b} \left[y^2\delta \frac{dL_i}{dy}\left(\sum_{j=1}^{3} a_j \frac{dL_j}{dy}\right) + y^2\kappa\phi_g^2 L_i \left(\sum_{j=1}^{3} \frac{da_j}{d\theta_g} L_j\right) + \frac{y^2\phi_g^2 L_i \left(\sum_{j=1}^{3} a_j L_j\right) r_i^{*2}}{1 + 6\phi_g^2 (r_i^* - (r_i^{*2}/r_i^{**}))} \right] dy \tag{22}$$
$$-L_i(y_a)Q_1^e - L_i\left(\frac{y_a + y_b}{2}\right)Q_2^e - L_i(y_b)Q_3^e = 0 \qquad i = 1,\ 2,\ 3$$

In matrix form in a typical element we have:

$$[K^e]\{a\} + [M^e]\left\{\dot{a}\right\} = Q^e \tag{23}$$

where

$$K_{ij}^e = \int_{y_a}^{y_b} \left(y^2\delta \frac{dL_i}{dy}\frac{dL_j}{dy} + \frac{y^2\phi_g^2 L_i L_j r_i^{*2}}{1 + 6\phi_g^2 (r_i^* - (r_i^{*2}/r_i^{**}))} \right) dy$$
$$i = 1,\ 2,\ 3 \quad j = 1,\ 2,\ 3 \tag{24}$$
$$(25) M_{ij}^e = \int_{y_a}^{y_b} y^2\kappa\phi_g^2 L_i L_j\, dy \quad i = 1,\ 2,\ 3 \quad j = 1,\ 2,\ 3$$

$$Q_1^e = \left(-y^2\delta\frac{dY}{dy}\right)_{y_a}, \quad Q_2^e = \left(y^2\delta\frac{dY}{dy}\right)_{((y_a+y_b)/2)^-} + \left(-y^2\delta\frac{dY}{dy}\right)_{((y_a+y_b)/2)^+}, \quad Q_3^e = \left(y^2\delta\frac{dY}{dy}\right)_{y_b} \tag{26}$$

The most commonly used scheme for the time approximation of Eq. (23) is the *α-family of approximation* in which a weighted average of the time derivatives at two consecutive time steps is approximated by linear interpolation of the values of the variable at two steps [23]:

$$a_{s+1} = a_s + \Delta\theta\dot{a}_{s+\alpha}$$
$$\dot{a}_{s+\alpha} = (1-\alpha)\dot{a}_s + \alpha\dot{a}_{s+1} \quad \text{for} \quad 0 \le \alpha \le 1 \tag{27}$$

For example when $\alpha=0$, Eq. (27) gives the *forward difference* approximation and when $\alpha=0.5$, Eq. (27) gives the Crank–Nicolson scheme which is used in this work.

Employing the *α-family of approximation*, Eq. (23) over a typical element becomes:

$$([M^e] + \Delta\theta\alpha[K^e])\{a^e\}_{s+1} = ([M^e] - \Delta\theta(1-\alpha)[K^e])\{a^e\}_s + \Delta\theta\{Q^e\} \tag{28}$$

Assembling Eq. (28) results:

$$[A]\{a\}_{s+1} = [B]\{a\}_s + \{Q\} \tag{29}$$

A, B are $2\times N+1$, $2\times N+1$ symmetric global known matrices and N is the number of mesh in the pellet domain (from the center up to surface of the spherical pellet). Assuming negligible external mass transfer resistance, the fluid concentration at the surface of the pellet is being known. Since there is not any point source or point sink in the domain of the problem, all of the components of the $\{Q\}$ are zero except the last component. Considering Eq. (15), all of the components of $\{a\}_0$ (the gas concentration vector at the initial time) are zero except the last component ($a(2\times N+1,\ 1)=1$).thus the system of equations (Eq. (29)) shall be condensed [23,24]. The resulting system of equations should be solved. Therefore the fluid concentration vector for the next time step becomes known. Simultaneously, since the fluid concentration is known at the initial time, Fourth order Runge–Kutta routine is used for solving Eq. (12). Thus the grain radius (or solid concentration) will be obtained for the same next time step. This procedure will be repeated until the final reaction time.

4. Results and discussion

In Fig. 1 results of this work are compared with the results of Shiravani et al. [25] (quantized method). In this figure, different values of the reaction Thiele modulus are considered. In Fig. 2 a comparison has been done between the results of this work with the results of Georgakis et al. [22] which is based on orthogonal collocation method. In this figure significant structural changes is considered while the accumulation parameter is about 0.001 (a gas–solid reaction). In addition to this, Eq. (9) is employed in this comparison (r^{*3} should be used instead of b in this equation). In Fig. 3 the variation of the porosity versus radius of the pellet is presented in case of considerable increase in the volume of the solid products with respect to the solid reactant. This figure shows the decrease of the porosity with the progress of the reaction. At $\theta_g=10.5$ this figure clearly shows that the porosity at the surface of the pellet becomes zero i.e. the surface of the solid reactant is completely blocked due to increase of the volume of the products ($Z=3.09$). In Fig. 4 the gas concentration versus radius of the pellet is presented in case of $Z=3.09$ at different times. In Fig. 5 comparison of this work with the orthogonal collocation solution of Prasannan et al.

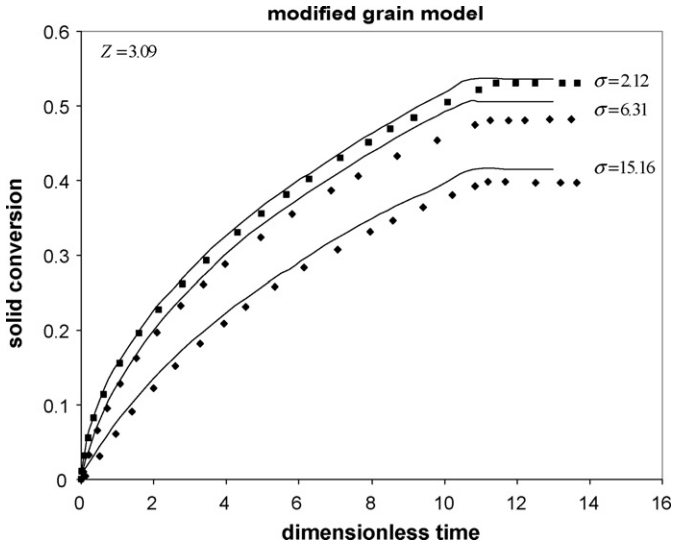

Fig. 1. Comparison of this work (continuous lines) with results of Shiravani et al. [25] (dotted points), $\sigma_g^2 = 38.8$, $\varepsilon_0 = 0.54$, $\kappa = 0.1$, $Sh = \infty$, employing Eq. (9).

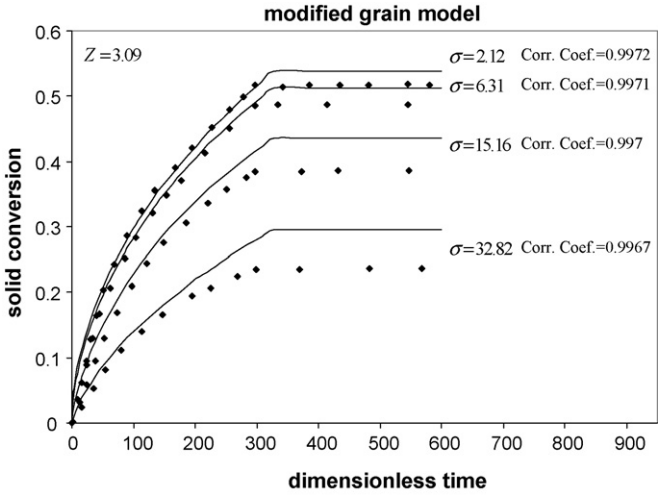

Fig. 2. Comparison of this work (continuous lines) with results of Georgakis et al. [22] (dotted points), $\sigma_g^2 = 38.8$, $\varepsilon_0 = 0.54$, $\kappa = 0.001$, $Sh = \infty$, $t(s) = \theta_g \times 30.07$, employing Eq. (9).

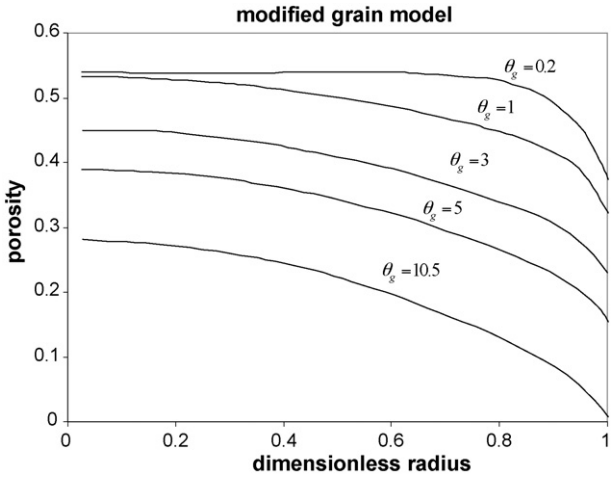

Fig. 3. Variation of the porosity along the pellet by the progress of reaction. $Z = 3.09$, $\sigma = 15.16$, $\sigma_g^2 = 38.8$, $\kappa = 0.001$, $Sh = \infty$, employing Eq. (9).

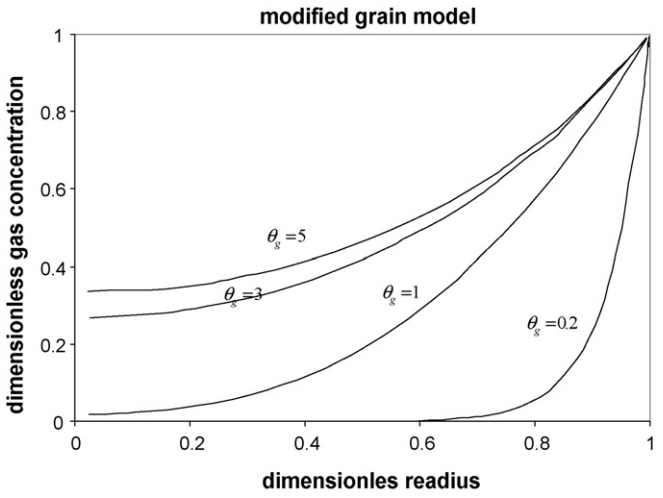

Fig. 4. Gas concentration profile versus radius of the pellet at different times. $Z = 3.09$, $\sigma = 15.16$, $\sigma_g^2 = 38.8$, $\kappa = 0.001$, $Sh = \infty$, employing Eq. (9).

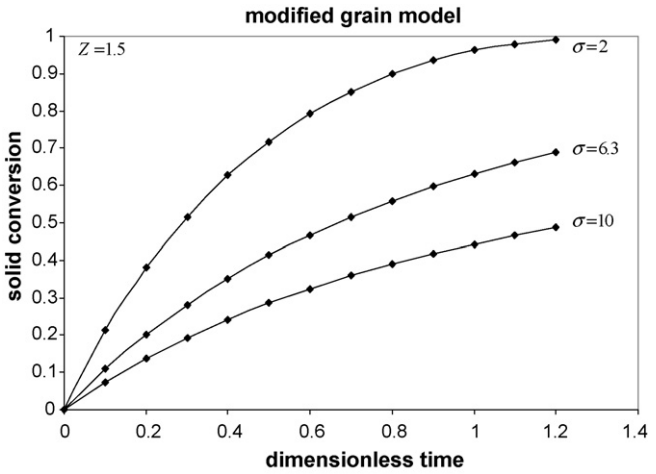

Fig. 5. Comparison of this work (continuous lines) with results of Prasannan et al. [26] (dotted points), $\sigma_g^2 = 0.167$, $\varepsilon_0 = 0.5$, $\kappa = 0.001$, $Sh = \infty$.

[26] is presented for different values of the reaction Thiele modulus. The accumulation parameter is about 0.001 (a gas–solid reaction) in this figure. In Fig. 6 comparison of the results of Bhatia [13] (random pore model) with this work in a liquid–solid reaction system ($\kappa = 0.5$) is presented. The comparison reveals complete agreement between the results. Moreover, the conversion–time results of a liquid–solid system for different values of Z and ϕ_r are presented in Figs. 7 and 8 respectively. These figures show the flexibility of Rayleigh–Ritz finite element method in the various reaction conditions. In Fig. 9 the variation of the porosity in random pore model for a liquid–solid system in case of significant structural changes ($Z = 3.09$) is depicted at different times. This figure shows that at $\theta_r = 1.9$, the porosity at the surface of the solid pellet becomes zero while the major parts of the solid pellet are still remaining inaccessible. This figure also reveals that in the presence of extreme fluid concentration gradient accompanied with structural changes, the major parts of the solid still completely unreacted. Finally in Fig. 10 application of the random pore model to predict the experimental data of Hartman and Coughlin [27] for the reaction of sulfur dioxide with limestone ($\kappa = 0.001$) at 1123 K (850 °C) for three different particle sizes is surveyed. The sulfation reaction proceeds rapidly in its early stages slow down as the time of exposure continues, and

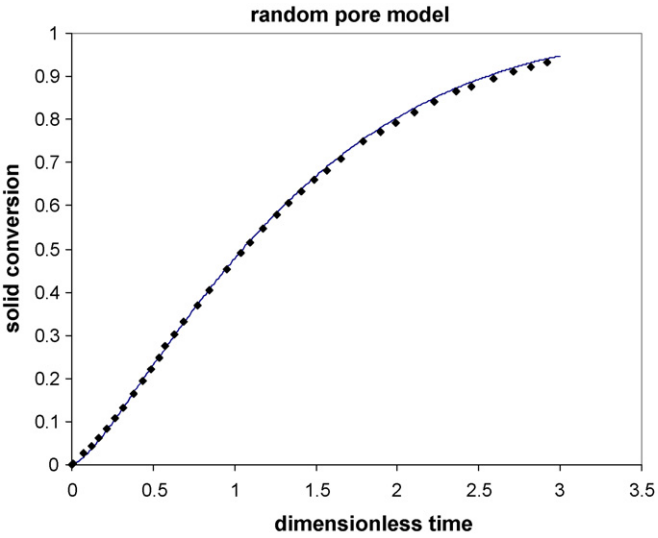

Fig. 6. Comparison of this work (continuous line) with the results of Bhatia [13] (dotted points) for a liquid–solid system. $\phi_r = 3$, $\psi = Z = 1$, $\beta = 0$, $\varepsilon_0 = 0.3$, $\kappa = 0.5$, $Sh = \infty$.

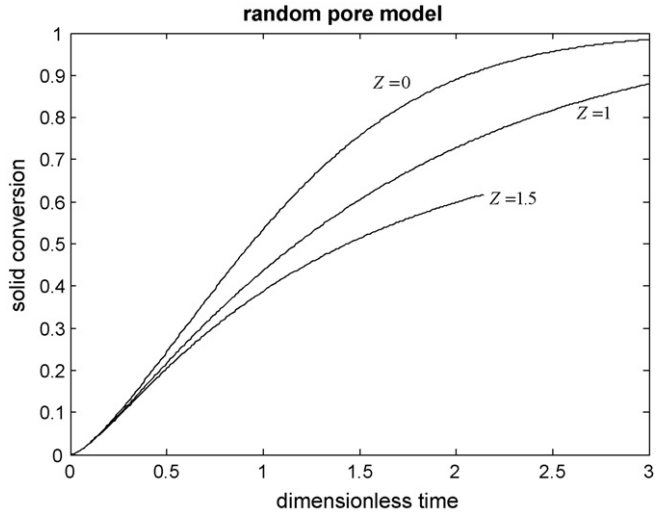

Fig. 7. Conversion–time curves in liquid–solid system for various values of Z. Parameters are: $\phi_r = 3$, $\psi = 1$, $\beta = 1$, $\varepsilon_0 = 0.3$, $\kappa = 0.5$, $Sh = \infty$.

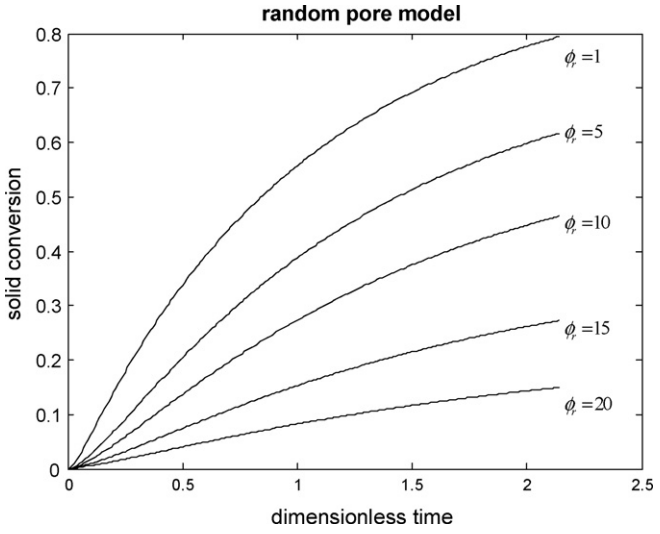

Fig. 8. Conversion–time curves in liquid–solid system for various values of ϕ_r. Parameters are: $Z = 1.5$, $\psi = 1$, $\beta = 1$, $\varepsilon_0 = 0.3$, $\kappa = 0.5$, $Sh = \infty$.

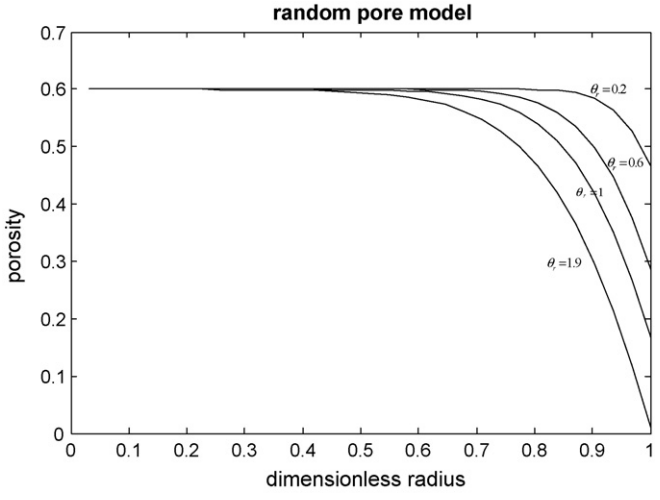

Fig. 9. Variation of the porosity in a liquid–solid system along the pellet by the progress of reaction. $Z = 3$, $\phi_r = 10$, $\psi = 1$, $\beta = 1$, $\varepsilon_0 = 0.6$, $\kappa = 0.5$, $Sh = \infty$.

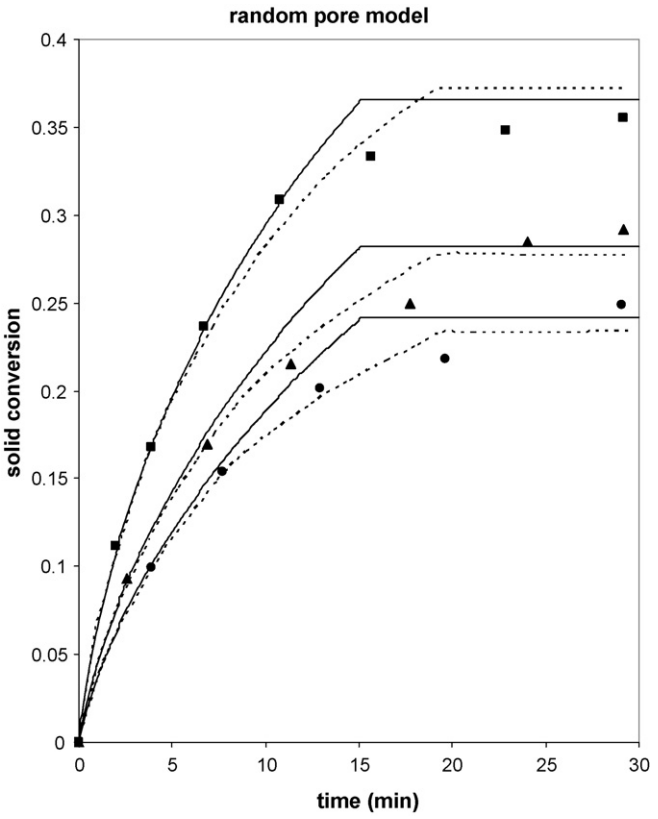

Fig. 10. Application of random pore model to experimental data of Hartman and Coughlin [27]. Continuous lines are the results of this work, dashed lines are the modeling of Bhatia and Perlmutter [12]. Parameters are: $Z = 3.09$, $\psi = 2.5$, $Sh = \infty$, $\varepsilon_0 = 0.52$, $M_B/\rho_B = 16.9\,\mathrm{cm^3/mol}$, $C_{Ag} = 3.2 \times 10^{-8}\,\mathrm{mol/cm^3}$, $\kappa = 0.001$, $\theta_r = 2.46t$ (min), $s_0 = 14.3 \times 10^4\,\mathrm{cm^2/cm^3}$, $k = 4.34\,\mathrm{cm^4/(mol\,s)}$, $\beta = 185$ ■ particle diameter 0.565 mm, ▲ particle diameter 0.9 mm, ● particle diameter 1.12 mm; corr. coeff. in case of particle dia. = 0.565 mm is 0.9971 for this work and is 0.993 for the results of Ref. [12]; corr. coeff. in case of particle dia. = 0.9 mm is 0.9905 for this work and is 0.993 for the results of Ref. [12]; corr. coeff. in case of particle dia. = 1.12 mm is 0.9385 for this work and is 0.940 for the results of Ref. [12].

the major portion of sulfur dioxide is sorbed by the solid particles during about the first 15 min of the reaction. Microscopic examination of this reaction revealed that the external surfaces of the sulfated samples were very smooth, while most of the pores were filled with the reaction product [27]. In this comparison, the effective diffusivity of the gas in the product layer (D_p) is the fitting parameter i.e. the value of the β (containing the D_p) was found by trial and error when the experimental data were fitted by the model. Fig. 10 shows the agreement between the computer code (this work) and experimental data at the best fit value of $\beta = 185$. The corresponding value of D_p to this level of β is $9.31 \times 10^{-13}\,\mathrm{m^2/s}$. Hartman and Coughlin [27] obtained the value of D_p to be $6 \times 10^{-13}\,\mathrm{m^2/s}$ in their work. The computer program also predicts the surface blockage time of the solid reactant to be about 15 min.

5. Conclusion

In this paper coupled nonlinear partial differential equations of fluid–solid reactions were numerically solved by Rayleigh–Ritz finite element method successfully. Comparison of the results of this work with other existing solutions for gas–solid systems and liquid–solid systems has been done in this effort. Results of this work predict the behavior of the reactions such as pore mouth closure (leading to incomplete solid conversion) successfully with considerable accuracy. Moreover, the results of liquid–solid reactions in the presence of extreme liquid concentration gradients

accompanied with significant structural changes in the solid reactant have been predicted very well.

Appendix A. Nomenclature

$a = C_A/C_{Ag}$ dimensionless fluid concentration
$b = C_B/C_{B0}$ dimensionless solid concentration
C_A fluid concentration in the pellet
C_{Ag} bulk fluid concentration
C_B solid concentration
C_{B0} initial solid concentration
D_e effective diffusivity of fluid A in the pellet
D_{e0} initial effective diffusivity of fluid A in the pellet
D_p effective diffusivity of fluid A in the product layer
F_p shape factor of the pellet = 1, 2, 3 for slab, cylinder and sphere, respectively
F_g shape factor of the grain = 1, 2, 3 for slab, cylinder and sphere, respectively
h length of an element
i,j position indexes
k reaction rate constant, cm/s for modified grain model, $cm^4/(mol\,s)$ for the random pore model respectively
M_A molecular weight of gaseous reactant
M_B molecular weight of solid reactant
M_D molecular weight of solid product
m distance from center of the pellet
r_g radius of unreacted core in the grain
r_{g0} initial grain radius
$r^* = r_g/r_{g0}$ dimensionless unreacted radius in the grain
R characteristic pellet length
S_0 reaction surface area per unite volume
s time index
Sh Sherwood number
T absolute temperature (K)
t time
X solid conversion
$y = m/R$ dimensionless position in the pellet
$\bar{y} = y - y_a$ local or element coordinate
ε pellet porosity
ε_0 initial pellet porosity
ρ_B true molar density of solid reactant B
ρ_D true molar density of solid product D
υ_B stoichiometric coefficient of solid reactant
$\kappa = \varepsilon_0 C_{Ag} M_B/\rho_B(1-\varepsilon_0)$ accumulation parameter
$\beta = 2k\rho_B(1-\varepsilon_0)/M_B D_p S_0$ product layer resistance
$\theta_g = kC_{Ag}M_B t/\rho_B r_{g0}$ dimensionless time for the modified grain model
$\theta_r = [kC_{Ag}S_0/(1-\varepsilon_0)]t$ dimensionless time for the random pore model
$\phi_r = R\sqrt{k\rho_B S_0/M_B D_{e0}}$ Thiele modulus for random pore model
$\sigma = R\sqrt{F_g k(1-\varepsilon_0)/D_e r_{g0}}$ reaction Thiele modulus for the pellet in the grain model
$\sigma_g = \sqrt{kr_{g0}/2D_p F_g}$ reaction modulus for the grain

References

[1] J. Szekely, J.W. Evans, H.Y. Sohn, Gas–Solid Reactions, Academic Press, New York, 1976.
[2] J. Szekely, C.I. Lin, H.Y. Sohn, A structural model for gas–solid reactions with a moving boundary. V. An experimental study of the reduction of porous nickel-oxide pellets with hydrogen, Chem. Eng. Sci. 28 (1973) 1975–1989.
[3] K.L. Breg, S.E. Olsen, Kinetics of manganese ore reduction by carbon monoxide, Met. Mater. Trans. B 31 (2000) 477–490.
[4] H. Ale Ebrahim, E. Jamshid, Kinetic study and mathematical modeling of the reduction of ZnO–PbO mixtures by methane, Ind. Eng. Chem. Res. 44 (2005) 495–504.
[5] S. Kimura, Oxidation kinetics of polycrystalline zinc sulfide grains, AIChE J. 35 (1989) 339–342.
[6] S. Zarkanitis, S.V. Sotirchos, Pore structure and particle size effect on limestone capacity for SO_2 removal, AIChE J. 35 (1989) 821–830.
[7] E.A. Efthimiadis, S.V. Sotirchos, Reactivity evolution during sulfidation of porous zinc oxide, Chem. Eng. Sci. 48 (1993) 829–843.
[8] A. Calvelo, J.M. Smith, Intrapellet transport in gas–solid non-catalytic reactions, in: Proceedings of the Chemca 70, Butterworth, Australia, 1971, Paper 3.1.
[9] O. Garza-Garza, M.P. Dadukovic, A variable size grain model for gas–solid reactions with structural changes, Chem. Eng. J. 24 (1982) 35–45.
[10] S.K. Bhatia, D.D. Perlmutter, A random pore model for fluid–solid reactions: I. Isothermal, kinetic control, AIChE J. 26 (1980) 379–386.
[11] S.K. Bhatia, D.D. Perlmutter, A random pore model for fluid–solid reactions. II. Diffusion and transport effects, AIChE J. 27 (1981) 247–254.
[12] S.K. Bhatia, D.D. Perlmutter, The effect of pore structure on fluid–solid reactions: application to the SO_2–lime reaction, AIChE J. 27 (1981) 226–234.
[13] S.K. Bhatia, On the pseudo steady state hypothesis for fluid solid reactions, Chem. Eng. Sci. 40 (1985) 868–872.
[14] G.R. Gavalas, A random pore model with application to char gasification at chemically controlled rates, AIChE J. 26 (1980) 577–585.
[15] G.R. Gavalas, Analysis of char combustion including the effect of pore enlargement, Cornbust. Sci. Technol. 24 (1981) 197–210.
[16] K. Hashimoto, P.L. Silveston, Gasification. I. Isothermal kinetic control model for a solid with a pore size distribution, AIChE J. 19 (1973) 259–268.
[17] K. Zygourakis, L. Arri, N.R. Amundson, Studies on the gasification of a single char particle, Ind. Eng. Chem. Fundam. 21 (1982) 1–12.
[18] P.G. Christman, T.F. Edgar, Distributed pore-size model for sulfation of limestone, AIChE J. 29 (1983) 388–395.
[19] A. Afshar Ebrahimi, H. Ale Ebrahim, M. Hatam, E. Jamshidi, Finite element solution for gas–solid reactions: application to the moving boundary problems, Chem. Eng. J. 144 (2008) 110–118.
[20] A. Afshar Ebrahimi, H. Ale Ebrahim, E. Jamshidi, Solving partial differential equations of gas–solid reactions by orthogonal collocation, Comput. Chem. Eng. 32 (2008) 1746–1759.
[21] N. Wakao, J.M. Smith, Diffusion in catalyst pellets, Chem. Eng. Sci. 17 (1962) 825–834.
[22] C. Georgakis, C.W. Change, J. Szekely, A changing grain size model for gas–solid reactions, Chem. Eng. Sci. 34 (1979) 1072–1075.
[23] J.N. Reddy, An Introduction to the Finite Element Method, McGraw-Hill, New York, 2006.
[24] J.N. Reddy, An Introduction to Nonlinear Finite Element Analysis, Oxford University Press, New York, 2004.
[25] A. Shiravani, E. Jamshidi, H. Ale Ebrahim, A new solution technique for fluid–solid reactions, Chem. Eng. J. 140 (2008) 246–277.
[26] P.C. Prasannan, P.A. Ramachandran, L.K. Doraiswamy, Gas–solid reactions: a method of direct solution for solid conversion profiles, Chem. Eng. J. 33 (1986), 462 19-25.
[27] M. Hartman, R.W. Coughlin, Reaction of sulfur dioxide with limestone and the grain model, AIChE J. 22 (1976) 490–498.